2020-07-29

Flowering poration a synergistic multi-mode antibacterial mechanism by a bacteriocin fold

Hammond, K

10.1016/j.isci.2020.101423
iScience
Elsevier BV

Journal Pre-proof

Flowering poration – a synergistic multi-mode antibacterial mechanism by a bacteriocin fold

Katharine Hammond, Helen Lewis, Samantha Halliwell, Florie Desriac, Brunello Nardone, Jascindra Ravi, Bart W. Hoogenboom, Mathew Upton, Jeremy P. Derrick, Maxim G. Ryadnov

PII: S2589-0042(20)30613-1

DOI: https://doi.org/10.1016/j.isci.2020.101423

Reference: ISCI 101423

To appear in: *ISCIENCE*

Received Date: 25 March 2020

Revised Date: 10 July 2020

Accepted Date: 27 July 2020

Please cite this article as: Hammond, K., Lewis, H., Halliwell, S., Desriac, F., Nardone, B., Ravi, J., Hoogenboom, B.W, Upton, M., Derrick, J.P, Ryadnov, M.G, Flowering poration – a synergistic multi-mode antibacterial mechanism by a bacteriocin fold, *ISCIENCE* (2020), doi: https://doi.org/10.1016/j.isci.2020.101423.

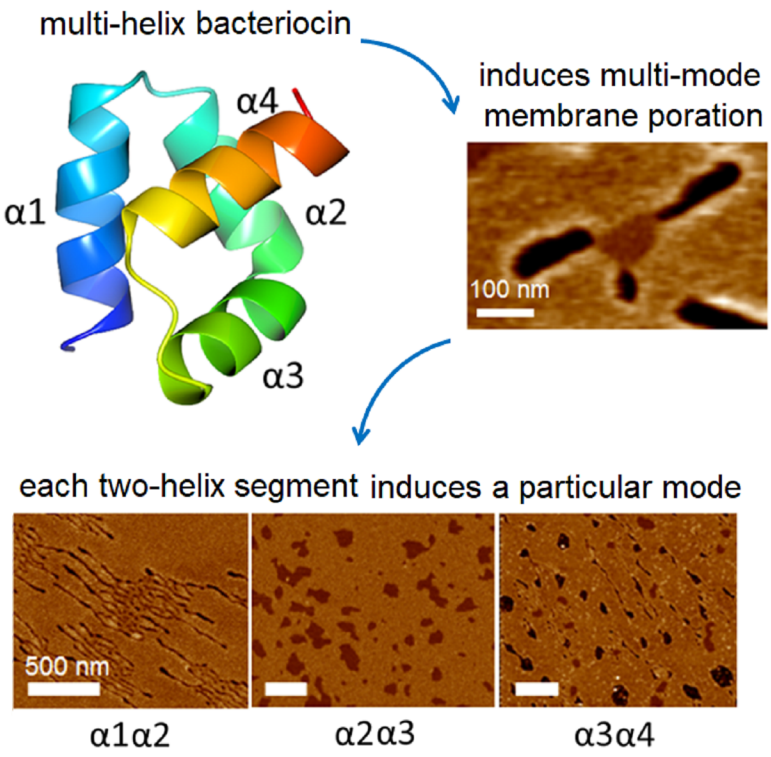

Flowering poration – a synergistic multi-mode antibacterial mechanism by a bacteriocin fold

Katharine Hammond,[1,2,3] *Helen Lewis,*[1] *Samantha Halliwell,*[4] *Florie Desriac,*[5] *Brunello Nardone,*[1] *Jascindra Ravi,*[1] *Bart W Hoogenboom*[2,3] *Mathew Upton,*[5] *Jeremy P Derrick*[4] *and Maxim G Ryadnov*[1,6,*,a]

[a] Lead Contact

[1]National Physical Laboratory, Hampton Road, Teddington, TW11 0LW, UK

[2]London Centre for Nanotechnology, University College London, London WC1H 0AH, UK

[3]Department of Physics & Astronomy, University College London, London WC1E 6BT, UK

[4]Lydia Becker Institute of Immunology and Inflammation, School of Biological Sciences, Faculty of Biology, Medicine and Health, Manchester Academic Health Science Centre, The University of Manchester, Oxford Road, Manchester, UK

[5]School of Biomedical Sciences, University of Plymouth, Plymouth, Devon, PL6 8BU, UK

[6]Department of Physics, King's College London, Strand Lane, London WC2R, UW

Corresponding author:

Dr Maxim G Ryadnov, National Physical Laboratory,

Hampton Road, Teddington, TW11 0LW, UK

Fax: (+44) 20 86140573; Tel: (+44) 20 89436078

max.ryadnov@npl.co.uk

SUMMARY: bacteriocins are a distinct family of antimicrobial proteins postulated to porate bacterial membranes. However, direct experimental evidence of pore formation by these proteins is lacking. Here we report a multi-mode poration mechanism induced by four-helix bacteriocins, epidermicin NI01 and aureocin A53. Using a combination of crystallography, spectroscopy, bioassays and nanoscale imaging, we established that individual two-helix segments of epidermicin retain antibacterial activity but each of these segments adopts a particular poration mode. In the intact protein these segments act synergistically to balance out antibacterial and hemolytic activities. The study sets a precedent of multi-mode membrane disruption advancing the current understanding of structure-activity relationships in pore-forming proteins.

INTRODUCTION

Host defense systems use pore-forming proteins to target pathogenic, host or aberrant cells (Parker and Feil, 2005). Bacteria secrete such proteins to access nutrients from the cells of their hosts or outcompete other bacteria living in the same environmental niches (Koehbach and Craik, 2019; Cotter et al., 2013), while human leukocytes release pore-forming proteins to kill pathogens (Iacovach et al., 2010). The spread of antimicrobial resistance has intensified interest in molecules promoting the lysis of microbial membranes with an emphasis on host defense peptides as potential anti-infectives (Lazar et al, 2018). These peptides favour attack on microbial membranes and each tends to support one poration mechanism. The adoption of different mechanisms within the same sequence can be tuned by careful site-directed mutations (Pfeil et al., 2018). This modulation is possible because host defence peptides adopt relatively simple conformations in membranes. For example, only a single, short helix is required to elicit strong antimicrobial effects (Koehbach and Craik, 2019). Bacteria themselves produce more complex antibacterial agents, termed bacteriocins, which specialize in killing closely related bacterial strains (Acedo et al., 2018). The killing is proposed to occur through membrane poration, although experimental evidence for this conjecture has yet to be reported (Hechard and Sahl, 2002).

Bacteriocins can be divided into subclasses according to their structural organisation and size (Arnison et al., 2013), with the most recent subclass represented by a multi-helix bundle group. Bacteriocins of this subclass are small proteins comprising several α-helices packing into compact globular structures. Unlike other bacteriocins that have post-translational backbone, side-chain modifications or operate as tertiary complexes, proteins from this subclass are leaderless, single-chain and cysteine-free (Cotter et al., 2013; Cotter et al., 2005).

Given that their structures are multi-helix folds, we reason that these proteins must induce multi-mode mechanisms of membrane disruption, with each mode supported by a specific constituent of their structure. Herein we validate this hypothesis, reporting the direct observation of multi-

mode membrane disruption by bacteriocins. We first determine a high-resolution crystal structure of epidermicin NI01 – a four-helix bacteriocin recently discovered in *S. epidermis* (Fig 1A) (Sandiford and Upton, 2012). We then synthesise individual constituents of this structure – two- and three-helix hairpins (Fig 1A and S1 in Supplemental Information) – characterise their biological and physical properties and compare them with those of the full-length epidermicin. Using atomic force microscopy, we demonstrate that each of helix-helix hairpins induces a distinct mode of membrane disruption in anionic phospholipid bilayers, whereas the intact protein combines all these modes into one synergetic mechanism which, to our knowledge, has not been observed before. We further demonstrate that this mechanism is not stereoselective as it is reproduced by the all-D version of NI01. We show that all tested structures are appreciably antimicrobial and that synergy between the different corresponding modes of membrane disruption balances out the antibacterial and hemolytic activities of the protein. Finally, we compare the disruption mechanisms of NI01 and another bacteriocin from the same fold group and find that the two mechanisms are strikingly similar sharing the same disruption modes.

RESULTS

NI01 folds into a four-helix bundle topology

The X-ray structure of NI01 revealed that it folds into a compact, four-helix bundle in which two α-hairpins are linked through a kink (φ = -116º and ψ = 36º) in the central helix at H25 (Fig 1B,C).

The transition between α1 and α2 is mediated by a type III β-turn, and from α3 to α4 by G36, which forms a break at the end of the third helix (Fig 1B, Table S1). The hydrophobic residues of all helices are buried in the core of the bundle, which is characteristic of bacteriocins and essential to stabilise the fold in solution. Aromatic residues account for 20% of all residues in this protein but are not engaged in the core. Instead, their side chains are locked in paired π-π interactions that appear to act as staples between spatially adjacent helices. Five pairs are formed

to support inter-helical crossovers, only two of which are formed between sequential helices, namely the F4-W23 and W32-W41 pairs that link α1 and α2, and α3 and α4 helices, respectively (Fig 1D). Four of the pairs involve the C-terminal helix (α4) including all of the remaining pairs, H25-W50, Y18-Y43 and F10-F39 (Fig 1E). Given that this helix is stapled with each of the other three helices, it may function as a leader helix, which synchronizes the insertion of NI01 into membranes. The central α2 and α3 helices share no aromatic pairs between them, which is expected for helices oriented perpendicular to one another, and is common for leaderless bacteriocins (Lohans et al, 2013). Finally, the analysis of the structure by PISA (Krissinel and Henrick, 2007) did not indicate any significant contacts between protein monomers indicating that the protein is monomeric in aqueous solution (Fig 1B).

NI01 folds cooperatively in solution and binds strongly to anionic membranes

Each helix in NI01 is at least two helical turns in length, which is sufficient to support the cooperative folding of the protein. Circular dichroism (CD) spectroscopy confirmed helix formation by NI01 in aqueous buffers (Fig 2A), with sigmoidal unfolding curves giving a single transition midpoint (T_M) of ~60 ºC (Fig 2B).

Denaturation was also fully reversible: the spectra collected before and after the thermal denaturation were nearly identical (Fig S2A). The signal intensity at 202 nm, which remained the same during denaturation provided a clear isodichroic point indicating a two-state transition between helical and unfolded forms (Fig S2B). However, even at temperatures as high as 90 ºC NI01 retained helical content: the spectral $\Delta\varepsilon_{222}/\Delta\varepsilon_{208}$ ratios for all spectra recorded during the thermal transition were ≥1, as expected for helical bundles (Fig 2A and S2B) (Kelly et al., 2005). The observation is consistent with the fact that NI01 retains antimicrobial activity following exposure to elevated temperatures (80 ºC), as reported elsewhere (Arnison et al., 2013). The helical content of the protein in aqueous buffers was comparable to that in aqueous 2,2,2-trifluoroethanol (TFE) (Fig S2C). Fluorinated alcohols promote intramolecular hydrogen bonding by excluding water from the solute and encompassing the polypeptide chain in a hydrophobic

"matrix" (Roccatano et al, 2002). Thus, the TFE-induced helix formation shows the extent to which an individual chain can fold into a helical state excluding supramolecular contributions. With no apparent changes at different TFE concentrations (Fig S2C), the helical content of NI01 was also independent of peptide concentrations (Fig S2D). Collectively, the results are indicative of a highly stable protein that is fully folded in solution.

Similar to other pore-forming proteins, which target bacteria, epidermicin is cationic having a net charge of +8 at neutral pH. In the crystal structure of NI01, polar side chains of each helix cluster on the exterior of the protein. In solution, the protein is a monodisperse particle of 2 nm in diameter exhibiting a high surface charge (ζ-potential of 20.8 ± 3.8 mV). These characteristics confer a high stability on the protein, allowing it to bind to anionic bacterial membranes as a monomer (Fig S3). Since NI01 is already folded in solution, CD spectroscopy could only reveal additive changes in helicity in membranes. As expected, the helical content for NI01 remained unchanged when it was measured in reconstituted phospholipid bilayers, which were constructed as unilamellar vesicles to mimic bacterial (anionic) and mammalian (zwitterionic) membranes (Fig S4A). Isothermal titration calorimetry (ITC) provided a more quantitative measure of protein-membrane interactions. Measured by titrating NI01 into anionic phospholipid membranes, binding isotherms revealed an exothermic process indicating enthalpy-driven ionic and hydrogen-bond interactions (Fig 2C). As protein-lipid ratios increased endothermic processes became more pronounced suggesting increasing contributions from hydrophobic interactions. This can be attributed to that the protein inserts deep into the hydrophobic interface of the bilayer (Fig 2C). The integrated heats fitted into a single site binding model gave a dissociation constant (K_D) of 0.3 μM with a ΔG of -8.9 kcal/mol, both values consistent with the characteristics of membrane-targeting antibiotics and pore-forming proteins (Seelig, 2004; Khatib et al., 2016). The biphasic binding found during the titrations suggests a synergistic, multi-mode mechanism by which NI01 selectively targets bacterial membranes. No binding was detected in zwitterionic phospholipid membranes (Fig S4B), consistent with negligible levels of toxicity towards

mammalian cells lines (Sandiford and Upton, 2012) and erythrocytes (Table S2). It can thus be concluded that the protein selectively disrupts bacterial membranes by binding to their surfaces through charge interactions and then re-arrangement into pores or channels.

NI01 induces a synergistic, multi-mode poration mechanism in anionic membranes

We probed the mechanism of membrane disruption by visualizing the effect of NI01 on reconstituted membranes using time-resolved atomic force microscopy in aqueous buffers (in-liquid AFM). The membranes of the same lipid composition used for the biophysical measurements in solution were deposited on mica surfaces as supported lipid bilayers (SLBs) (Rakowska et al., 2013). The resulting preparations yield flat (to within ≤0.1 nm) fluid-phase membranes that allow for accurate depth measurements of surface changes (Lin et al., 2006; Mingeot-Leclercq et al., 2008). Within minutes NI01 formed floral patterns on the SLBs. These patterns comprised roughly circular patches of thinned membranes radially propagating with petal-like lesions or pores (Fig 3A, S5A). Most patterns had three petals per patch (Fig 3B). The patches were ~2 nm in depth half-way through the bilayer, which is consistent with membrane thinning effects commonly observed for antimicrobial peptides (Pfeil et al., 2018). In contrast, the petal-like lesions extended all the way across the membrane (4 nm), i.e. were transmembrane pores (Fig 3C). The lesions were tapered at one end connecting with their respective patches, whereas the opposite end appeared as a growing circular pore merging with other pores (Figs 3D, E and S5A). Complementary to the ITC results, the AFM measurements showed that the bacteriocin was selective towards bacterial membranes. No changes could be detected in SLBs mimicking mammalian membranes, even at higher concentrations (Fig S5B).

The patches of thinned membranes appear as contact regions from which NI01 radially diffuses into the lipid matrix. This scenario resembles mechanisms proposed for four- and five-helix protein toxins that insert into the upper leaflet of the bilayer where they arrange into pores (González et al, 2000; Michalek et al., 2013). Similarly, antimicrobial peptides accumulate in the upper leaflet causing the thinning of phospholipid bilayers (Heath et al., 2018). These studies

indicate that as more peptide binds to the bilayers thinning areas grow in size but not in depth, as also observed for NI01 (Fig 3E) (Mecke et al., 2005). This suggests that a portion of NI01 should specialize in binding to the upper leaflet and be plastic enough to orchestrate protein re-assembly into pores. β-hairpins and bent α-helices are common folding topologies that induce membrane thinning and exfoliation (Jang et al., 2006; Pyne et al., 2017). NI01 has three overlapping helical hairpins (Fig 1A). The two terminal hairpins have similar up-and-down topologies, in which individual helices are clearly separated by extended turns (Fig 1B). With the N- and C-terminal helices being twice the length of the central helices, the terminal hairpins have the capacity for transmembrane insertion. In contrast, the two central helices are arranged into an α-α corner via a kink at an obtuse angle, which constrains the helices into a more open hairpin conformation (Figs 1B and S6). A boomerang-like shape of this hairpin could make it lie flat on membrane surfaces, favouring membrane thinning over transmembrane poration (Fig S6).

Each mode of the mechanism is activated by a specific two-helix segment of NI01

To gain more insight into these predictions, all three hairpins - α1α2, α2α3 and α3α4 (Fig 1A), were synthesised (Fig S1), characterised (Fig S7) and imaged by AFM on SLBs (Fig 4). The first two hairpins showed strikingly distinctive behaviours, each supporting exclusively one mode of the mechanism observed for NI01 (Fig 4).

The first hairpin, α1α2, formed extended petal-like pores that ran parallel to each other without branching. The regions of thinned membranes that in NI01 served as branching points for the pores were absent in SLBs treated with α1α2. In contrast, membrane thinning was apparent in SLBs treated with α2α3, with no indication of transmembrane pores. Although the regions imaged for α2α3 were similar in size and morphology to those formed by NI01, the petal-like pores of α1α2 appeared thinner and more extended when compared to those of NI01 (Fig 4). Wide, circular pores were dominant in SLBs treated with α3α4, with membrane-thinning patches being also abundant, which together indicate that α3α4 induced a mixed mode of membrane disruption (Fig 4).

In these experiments, it is evident that membrane thinning patches occur only when α3 is present (Fig 4). Both α2α3 and α3α4 incorporate this helix and α3α4 is the only of the three hairpins that induces the two membrane rupture modes. Thus, α3 appears to support the interplay of rupture modes favoured by other helices. Further evidence for this was derived from the behaviour of the two terminal three-helix hairpins, which were also produced as individual sequences (Fig S1). The N-terminal hairpin (α1α2α3) should combine two rupture modes: transmembrane lesions of α1α2 and thinned patches of α2α3, but without the synergy characteristic of NI01 manifesting in the conserved combined patterns of thinned patches and petals. For the C-terminal three-helix hairpin (α2α3α4) membrane thinning is expected to dominate as the synergy was already lacking in α3α4, and α2α3 did not form transmembrane pores. Consistent with this reasoning, the two predicted modes of membrane disruption were evident for α1α2α3 (Fig S8A). Although circular transmembrane pores could be detected for α2α3α4, these were much smaller in size, which contrasted with the abundance of thinned membrane regions caused by this hairpin (Fig S8A). The two three-helix hairpins were partially folded in solution, indicating impaired cooperativity of folding in solution when compared to that of NI01 (Fig S8B). Comparable helical content in solution was recorded for α3α4, which is notable given that α1α2 and α2α3 were unfolded (Fig S7). As for these two-helix hairpins, helicity sharply increased upon membrane binding for the terminal hairpins (Figs S7, 8B) The results indicate that two- and three-helix hairpins containing α3 form membrane thinning patches, which emphasizes the mediatory role of this helix in supporting the interplay of the different modes of membrane disruption.

The C-terminal helix, α4, is the only helix in NI01 interacting with all other helices via the aromatic pairs. It is also a part of α3α4, which is the only two-helix hairpin that folds in solution (Fig 1). In α2α3α4, α2 and α3 share no single aromatic pair between them. H25 is an exception in that it is located in the central turn connecting the two helices. The residue forms an aromatic pair with the terminal W50, which appears important for directing the insertion of α4. In addition, H25 is cationic, suggesting that it may bind to anionic lipids. Indeed, in both crystal forms H25

was observed to bind to SO^{2-}_4 (Fig S9). In antimicrobial peptides similar electrostatic interactions are formed between phosphate groups and cationic residues, which in NI01 are represented by lysine (Fig 1A). Consistent with the exothermic phase in the ITC measurements (Fig 2C), the residue displaces water from the phosphate and strongly binds to it. The formed interactions are strong enough for membrane binding and cooperative enough to allow different disruption modes to manifest in synergy, one distinctive, conserved mechanism.

To test these conventions, all lysines were replaced with arginines in an all-arginine mutant of NI01, R-NI01 (Fig 1A). Unlike lysine, arginine is positively charged at all stages of membrane binding and insertion and traps more phosphate and water by providing five hydrogen-bond donors (Li et al., 2013). This difference manifests in a tighter binding to membrane surfaces, and, as shown elsewhere, limits protein insertion into the upper leaflet of the bilayer (Pyne et al., 2017). Replacing H25 with arginine preserves the positive charge in the site, but also eliminates the H25-W50 pair compromising cooperativity in interactions between helices and the ability of α4 to insert. Indeed, this mutant produced exclusively thinning patches in the membranes, which were strikingly similar to those observed for α2α3 (Figs 4 and S10A). Furthermore, R-NI01 was 50% less helical than NI01 (Fig S10B). The loss in helicity was restored upon binding to phospholipid membranes (Fig S10B). This behaviour was similar to that of the three-helix hairpins, which were considerably less helical in solution than NI01, but whose helical content increased in membranes (Fig S8B). These results indicate that this mutation had a detrimental effect on NI01 folding in solution and its multi-mode mechanism in membranes.

The importance of these findings is two-fold. Firstly, the analysis of disruption mechanisms by individual hairpins confirm that NI01 exhibits a conserved, synergistic mechanism of membrane disruption. This is ensured by the cooperative folding of NI01 and tertiary contacts of its constituent helices. Each of these helices makes an important contribution to the complex pattern of this mechanism, but none of them is sufficient individually. Secondly, all hairpin derivatives disrupt bacterial mimetic membranes. This suggests that all of the hairpins are antimicrobial and

that their antimicrobial activities do not require a specific receptor to target bacteria, and therefore the antimicrobial activity of NI01 is not stereoselective.

Synergy in the multi-mode mechanism determines the biological selectivity of the protein

Considering the first point, NI01 and all of its derivatives exhibited comparable levels of antibacterial activity. Minimum inhibitory concentrations (MICs) were similar to those obtained for conventional antibiotics (Table S2). Noteworthy differences were observed in MICs for Gram-positive *S. aureus* and Gram-negative *P. aeruginosa*. NI01, α1α2 and α3α4 were equally effective against *S. aureus* and ineffective against *P. aeruginosa*. Intriguingly, α2α3 showed a reversed trend, which may be attributed to differences in the cell-wall structure of the bacteria. The peptidoglycan layer of Gram-positive cells is rich in anionic teichoic polymers, which might prevent α2α3 from reaching the cytoplasmic membrane (Yeaman and Yount, 2003). This proposition is supported by the observation that α2α3 remained largely unfolded in membranes and hence is subject to conformational fluctuations caused by binding to the teichoic polymers (Fig S7). All other hairpins and R-NI01 responded to membrane binding with sharp increases in helicity. Other Gram-positive bacteria, *B. subtilis* and *M. luteus*, proved to be susceptible to all of the NI01 derivatives used (Table S2). Peptidoglycans in these bacteria undergo continuous transformations from thick to thin layers, which makes their membranes more vulnerable to the attack by α2α3 (Tocheva et al., 2013; Vollmer, 2008). Consistent with the lack of activity against *S. aureus*, α2α3 failed to affect methicillin-resistant *S. aureus* (MRSA) strains. NI01 and the other two-helix hairpins maintained similar levels of activity against these pathogens when compared to those for the susceptible strain (Tables S2&3). The three-helix hairpins were less active against MRSA. Both these hairpins incorporate α2α3 that was inactive against any of the *S. aureus* strains tested. Therefore, the impact of thicker peptidoglycan layers of MRSA (García et al, 2013), on their activity is expected to be greater (Tables S2& S3). Another notable trend was observed for Gram-negative bacteria. NI01 and its derivatives appeared to be active only against *E. coli*. Similar to peptidoglycan layers in Gram-positive bacteria, lipopolysaccharide (LPS)

layers represent a key virulence factor for Gram negative membranes. To probe this, two additional *E. coli* strains were tested: a short-chain LPS or rough strain, SBS363, and a smooth strain comprising full-length, mature O-chains, ML35 (Ebbensgaard et al., 2018). All derivatives were active against the rough, more susceptible type, but the smooth type was resistant to all two-helix hairpins, except α1α2 (Table S3).

Considering the second point, NI01 was re-made into an all-D form (Fig S1). The protein adopted helical conformations that quantitatively mirrored those of the wild-type all-L NI01 in both solution and membranes (Figs 2A and S4A). In bacterial membranes the all-D form revealed a strikingly similar pattern to that of the all-L form (Fig S11), and both epimeric forms exhibited comparable antibacterial activities across all bacteria and strains tested (Tables S2 & S3). Taken together the results of these biological tests confirmed the antibacterial properties of NI01, with stronger activities observed for the derivatives exhibiting transmembrane disruption modes.

Bacteriocins, unlike host defence peptides or helminth defence molecules (Hammond et al., 2019), do not originate from multicellular organisms. However, there can be a selective pressure on bacteria residing in human hosts to remain in a commensal state. Consequently, bacteriocins produced by these bacteria should be able to differentiate between bacterial and host cells. For therapeutic applications, this requirement extends to red blood cells, which are weakly anionic and can also be targeted by bacteriocins. In this regard, NI01 proved to be non-hemolytic in both L- and D-forms at concentrations equivalent to >100 x MICs against Gram positive strains. This result was striking as all other derivatives caused appreciable hemolysis, except α2α3, which showed no hemolytic activity even at high concentrations (>600 µg/mL). These findings suggest that this hairpin re-balances antibacterial and hemolytic activities of NI01 by effectively diminishing the impact of the terminal helices, which favour transmembrane poration. Hemolytic activities drastically increased for R-NI01 and other hairpins, all of which lack the synergy of inter-helix interactions characteristic for NI01. As a consequence, these derivatives were incapable to differentiate between bacterial and erythrocytic membranes.

Mechanistic similarities with other four-helix bacteriocins

To this end, we have shown that NI01 exhibits a unique multi-mode mechanism of membrane disruption. To the best of our knowledge, this is also the first direct observation of bacteriocin-induced poration, which prompts an obvious comparison with other bacteriocins.

With this in mind, we performed a similar analysis for aureocin A53 (Fig 5A). This bacteriocin belongs to the same four-helix bundle group and its structure was recently solved by NMR spectroscopy (Fig 5B) (Acedo et al., 2016). As gauged by CD spectroscopy, the protein folded remarkably similar to that of NI01, with the two proteins having a nearly identical helical content (Fig 5C). A53 was as stable as NI01 with (T_M) of ~54 ºC (Fig S12A), folded reversibly and independently of concentration (Fig S12B, C), and showed no changes at increasing TFE concentrations (Fig S12D). BLAST searches indicated a significant level of sequence homology between the two proteins (38% identity). The location and extent of turn regions and individual helices were also very similar, while hydrophobic, polar and aromatic residues were well conserved (Fig 5A). Outside of the identity regions the exact sequence compositions of NI01 and A53 are different. Despite that the observed structural similarities suggest that A53 might exhibit a similar mechanism of membrane disruption.

AFM analyses of A53-treated anionic membranes showed disruption modes similar to those recorded for NI01: membrane thinning patches and transmembrane lesions and pores (Fig 5D). The patches were more extended than those for NI01. The petal-like lesions were morphologically similar to those of NI01, also ending with circular pores and grew out of the patches. Depth profiles for each mode were identical for the two bacteriocins (Figs 3C & 5E). Overall, the same characteristics of membrane disruption were evident for both proteins, which exhibited the same folding topology, sequence length and helical content. The variations in the mechanisms may be attributed to amino-acid permutations in helical and turn regions of the two proteins.

DISCUSSION

Bacteriocins have long been recognized as highly specific antibiotics that bacteria develop to outcompete closely related strains. It has also been long thought that these small proteins act by porating bacterial membranes like other pore-forming toxins, some antibiotics and host-defense peptides (Hechard and Sahl, 2002) However, direct evidence for bacteriocin-promoted poration has been lacking, despite the fact that bacteriocins belong to a distinctive family of host defence molecules with a common protein fold (Cotter et al., 2013; Acedo et al., 2018; Hechard and Sahl, 2002). Although several bacteriocin structures have been solved (Lohans et al., 2013; González et al., 2000; Acedo et al., 2016), the way their structural features specify antimicrobial mechanisms remains obscure. This study partially filled this gap by solving the fold of an archetypal bacteriocin, epidermicin NI01, and correlating it with a unique mechanism comprising several distinctive modes of membrane disruption, in contrast to alternative scenarios that assume one poration mode per membrane-disrupting agent. Furthermore, we experimentally demonstrated that it is the cooperativity of interactions between the structural constituents, helical hairpins, which orchestrates multiple modes into one synergistic process. For example, the central hairpin, α2α3, was found to have a direct and reciprocal impact on the terminal helices translating different disruption modes into one dynamic process. This mechanism is conserved, favors anionic membranes and is not stereoselective. Thinning patches and transmembrane petals tended to expand with time, whereas their morphology and depths did not change. This type of propagation is likely to occur at the expense of NI01 monomers oligomerizing on and in the lipid bilayers. Similarly, the transition from a patch to a lesion is likely to involve an oligomerization event. Existing models of membrane disruption by pore-forming proteins suggest that these proteins associate via their hydrophobic surfaces that become exposed as their cationic surfaces face anionic lipids (González et al., 2000; Michalek et al., 2013; Acedo et al., 2016). The models appear universal for proteins adopting four- and five-helix folds: acanthaporin produced by pathogenic amoebae, natural killer cell lysins and bacteriocins analogous to NI01 and A53 may

have different biological functions, but all share similar characteristics of high stability, surface charge and conserved folding and hence may disrupt membranes via similar mechanisms. It remains unclear however if membrane disruption involves a minimal, active oligomer which defines the size and dynamics of the forming pores, as was shown for single-helix antimicrobial peptides (Pyne et al., 2017).

To sum up, our results revealed that the four-helix bundle organisation of bacteriocins is necessary to complete such a highly regulated and sophisticated mechanism. The fold itself encodes this decisively physical means of selective membrane attack that is likely to hold true for other single-chain bacteriocins. The behaviour of another four-helix bacteriocin, A53, supports this conclusion.

LIMITATIONS OF THE STUDY

The exact reason for this complex mechanism is unclear. One possibility is that four-helix folds may better adapt to overcome a wide range of resistant membranes. The subtlety with which constituent helices cooperate is what makes bacteriocins less susceptible to acquired antibacterial resistance. This contrasts with host-defense peptides and membrane-active antibiotics that rely on a single disruption mode and are less fit against emerging strategies of membrane resistance (Needham and Trent, 2013). Another question is whether a multi-mode membrane disruption constitutes a common hallmark of bacteriocins, which may distinguish these proteins from other pore-forming and antibacterial molecules. Extensive site-directed mutagenesis of bacteriocin sequences together with AFM analysis of their action on bacterial membranes may provide additional insights into the mechanism. These proposals merit further independent investigations.

RESOURCE AVAILABILITY

Lead contact

Maxim G Ryadnov

max.ryadnov@npl.co.uk

Materials Availability

This study did not generate new unique reagents.

Data and Code Availability

The data supporting the findings of this study is available within this paper and its supplemental information. Coordinates and structure factors generated during this study are deposited in PDB with the accession codes 6SIF ($P2_12_12$) and 6SIG (*C222*).

ACKNOWLEDGEMENTS

We acknowledge funding from the UK's Department for Business, Energy and Industrial Strategy, Innovate UK (grant: 103358), and the UK's Biotechnology and Biological Sciences, and Medical Research Councils (BBSRC and MRC grants: BB/N015487/1, BB/J021474/1 and MR/R000328/1).

AUTHOR CONTRIBUTINOS

All authors designed the experiments, analysed and interpreted the data. K. H., H. L., S. H., F. D., B. N. and J. R. performed the research. B. W. H., M. U., J. P. D. and M. G. R. supervised the research. M. G. R wrote the manuscript. All authors contributed to the editing of the manuscript.

DECLARATION OF INTERESTS

A patent application has been filed on the subject matter of the manuscript.

REFERENCES

Acedo, J. Z., Chiorean, S., Vederas, J. C., and van Belkum, M. J. (2018). The expanding structural variety among bacteriocins from Gram-positive bacteria. FEMS Microbiol. Rev. 42, 805-828.

Acedo, J. Z., van Belkum, M. J., Lohans, C. T., Towle, K. M., Miskolzie, M., and Vederas, J. C. (2016). Nuclear magnetic resonance solution structures of lacticin Q and aureocin A53 reveal a structural motif conserved among leaderless bacteriocins with broad-spectrum activity. Biochemistry 55, 733-742.

Arnison, P. G., Bibb, M. J., Bierbaum, G., Bowers, A. A., Bugni, T. S., Bulaj, G., Camarero, J. A., Campopiano, D. J., Challis, G. L., Clardy, J., et al. (2013). Ribosomally synthesized and post-translationally modified peptide natural products: overview and recommendations for a universal nomenclature. Nat. Prod. Rep. 30, 108-160.

Cotter, P. D., Hill, C., and Ross, R. P. (2005). Bacteriocins: developing innate immunity for food. Nat. Rev. Microbiol. 3, 777–788.

Cotter, P. D., Ross, R. P., and Hill, C. (2013). Bacteriocins – a viable alternative to antibiotics? Nat. Rev. Microbiol. 11, 95-105.

Ebbensgaard, A., Mordhorst, H., Aarestrup, F. M., and Hansen, E. B. (2018). The role of outer membrane proteins and lipopolysaccharides for the sensitivity of *Escherichia coli* to antimicrobial peptides. Front Microbiol. 9, 2153.

García, A. B., Viñuela-Prieto, J. M., López-González L., and Candel, F. J. (2017). Correlation between resistance mechanisms in *Staphylococcus aureus* and cell wall and septum thickening. Infect Drug Resist. 10, 353–356.

González, C., Langdon, G. M., Bruix, M., Gálvez, A., Valdivia, E., Maqueda, M., and Rico, M. (2000). Bacteriocin AS-48, a microbial cyclic polypeptide structurally and functionally related to mammalian NK-lysin. Proc. Natl. Acad. Sci. USA 97, 11221-11226.

Hammond, K., Lewis, H., Faruqui, N., Russell, C., Hoogenboom, B. W., and Ryadnov, M. G. (2019). Helminth defense molecules as design templates for membrane active antibiotics. ACS Infect Dis. 5, 1471-1479.

Heath, G. R., Harrison, P. L., Strong, P. N., Evans, S. D., and Miller, K. (2018). Visualization of diffusion limited antimicrobial peptide attack on supported lipid membranes. Soft Matter 14, 6146-6154.

Hechard, Y., and Sahl, H. G. (2002). Mode of action of modified and unmodified bacteriocins from Gram positive bacteria. Biochimie 84, 545-557.

Iacovach, I., Bischofberger, M., and van der Goot, F. G. (2010). Structure and assembly of pore-forming proteins. Curr. Opin. Struct. Biol. 20, 241-216.

Jang, H., Ma, B., Woolf, T. B., and Nussinov, R. (2006). Interaction of protegrin-1 with lipid bilayers: membrane thinning effect. Biophys. J 91, 2848-2859.

Kelly, S. M., Jess, T. J., and Price, N. C. (2005). How to study proteins by circular dichroism. Biochim. Biophys. Acta, Proteins Proteomics 1751, 119–139.

Khatib, T. O., Stevenson, H., Yeaman, M. R., Bayer, A. S., and Pokorny, A. (2016). Binding of daptomycin to anionic lipid vesicles is reduced in the presence of lysyl-phosphatidylglycerol. Antimicrob. Agents Chemother. 60, 5051-5053.

Koehbach, J., and Craik, D. J. (2019). The vast structural diversity of antimicrobial peptides. Trends Pharmacol. Sci. 40, 517-528.

Krissinel, E., and Henrick, K. (2007). Inference of macromolecular assemblies from crystalline state. J. Mol. Biol. 372, 774–797.

Lazar, V., Martins, A., Spohn, R., Daruka, L., Grézal, G., Fekete, G., Számel, M., Jangir, P. K., Kintses, B., Csörgő, B., et al. (2018). Antibiotic-resistant bacteria show widespread collateral sensitivity to antimicrobial peptides. Nat. Microbiol. 3, 718-731.

Li, L., Vorobyov, I. and Allen, T. W. (2013). The different interactions of lysine and arginine side chains with lipid membranes. J Phys Chem B 117, 11906-11920.

Lin, W.-C., Blanchette, C. D., Ratto, T. V., and Longo, M. L. (2006). Lipid asymmetry in DLPC/DSPC-supported lipid bilayers: a combined AFM and fluorescence microscopy study. Biophys. J. 90, 228–237.

Lohans, C. T., Towle, K. M., Miskolzie, M., McKay, R. T., van Belkum, M. J., McMullen, L. M., and Vederas, J. C. (2013). Solution structures of the linear leaderless bacteriocins enterocin 7A and 7B resemble carnocyclin A, a circular antimicrobial peptide. Biochemistry 52, 3987-3994.

Mecke, A., Lee, D. K., Ramamoorthy, A., Orr, B. G., and Banaszak Holl, M. M. (2005). Membrane thinning due to antimicrobial peptide binding: an atomic force microscopy study of MSI-78 in lipid bilayers. Biophys. J 89, 4043-4050.

Michalek, M., Sönnichsen, F. D., Wechselberger, R., Dingley, A. J., Hung, C. W., Kopp, A., Wienk, H., Simanski, M., Herbst, R., Lorenzen, I. et al. (2013). Structure and function of a unique pore-forming protein from a pathogenic acanthamoeba. Nat. Chem. Biol. 9, 37-42.

Mingeot-Leclercq, M.-P., Deleu, M., Brasseur, R., and Dufrêne, Y. F. (2008). Atomic force microscopy of supported lipid bilayers. Nat. Protoc. 3, 1654−1659.

Needham, B. D., and Trent, M. S. (2013). Fortifying the barrier: the impact of lipid A remodeling on bacterial pathogenesis. Nat. Rev. Microbiol. 11, 467–481.

Parker, M. W., and Feil, S. C. (2005). Pore-forming protein toxins: from structure to function. Prog. Biophys. Mol. Biol. 88, 91–142.

Pfeil, M. P., Pyne, A. L. B., Losasso, V., Ravi, J., Lamarre, B., Faruqui, N., Alkassem, H., Hammond, K., Judge, P. J., Winn, M., et al. (2018). Tuneable poration: host defense peptides as sequence probes for antimicrobial mechanisms. Sci. Rep. 8, 14926.

Pyne, A., Pfeil, M. P., Bennett, I., Ravi, J., Iavicoli, P., Lamarre, B., Roethke, A., Ray, S., Jiang, H., Bella, A. et al. (2017). Engineering monolayer poration for rapid exfoliation of microbial membranes. Chem. Sci. 8, 1105–1115.

Rakowska, P. D., Jiang, H., Ray, S., Pyne, A., Lamarre, B., Carr, M., Judge, P. J., Ravi, J., Gerling, U. I., Koksch, B., et al. (2013). Nanoscale imaging reveals laterally expanding antimicrobial pores in lipid bilayers. Proc. Natl. Acad. Sci. USA 110, 8918–8923.

Roccatano, D., Colombo, G., Fioroni, M., and Mark, A. E. (2002). Mechanism by which 2,2,2-trifluoroethanol/water mixtures stabilize secondary-structure formation in peptides: A molecular dynamics study. Proc. Natl. Acad. Sci. USA 99, 12179–12184.

Sandiford, S., and Upton, M. (2012). Identification, characterization, and recombinant expression of epidermicin NI01, a novel unmodified bacteriocin produced by *Staphylococcus epidermidis* that displays potent activity against Staphylococci. Antimicrob. Agents Chemother. 56, 1539-1547.

Seelig, J. (2004). Thermodynamics of lipid-peptide interactions. Biochim. Biophys. Acta, Biomembranes 1666, 40-50.

Tocheva, E. I., López-Garrido, J., Hughes, H. V., Fredlund, J., Kuru, E., Vannieuwenhze, M. S., Brun, Y. V., Pogliano, K., and Jensen, G. J. (2013). Peptidoglycan transformations during *Bacillus subtilis* sporulation. Mol. Microbiol. 88, 673–686.

Vollmer, W. Structural variation in the glycan strands of bacterial peptidoglycan. (2008). FEMS Microbiol. Rev. 32, 287-306.

Yeaman, M. R., and Yount, N. Y. (2003). Mechanisms of antimicrobial peptide action and resistance. Pharmacol. Rev. 55, 27–55.

MAIN FIGURE TITLES AND LEGENDS

Figure 1. The structure of NI01. (A) Primary structure of NI01 and its derivatives – two-helix and three-helix hairpins, and an arginine mutant, R-NI01. Coloured staples indicate π-π interactions between aromatic residues of different helices, labelled α1-α4. Turns are underlined in the sequences. Arginine residues in R-NI01 are shown in blue. (B) Crystal structure of NI01. Ribbon representation from the N-terminus (blue) to the C-terminus (red). (C) Stick representation of the central kink linking two terminal hairpins at H25. (D) Two aromatic pairs, F4-W23 and W32-W41, between sequential helices: α1α2, and α3α4, respectively. (E) Remaining three aromatic pairs, all involving the C-terminal helix, H25-W50, Y18-Y43 and F10-F39.

Figure 2. NI01 folding. (A) CD spectra for NI01 (blue line) and its all-D form (20 μM protein) in 10 mM phosphate buffer (black line). (B) Thermal unfolding curve and its first derivative highlighting a single transition point (T_M). (C) Isothermal titration calorimetry of NI01 (500 μM) binding to bacterial mimetic membranes. Heat absorbed (μcal/s) for each isotherm is plotted versus titration time (upper panel). Integrated heats (kcal/mol) are plotted versus protein-lipid molar ratios (lower panel), showing a curve fitting to a one-set binding model (black line).

Figure 3. In liquid AFM imaging of reconstituted bacterial membranes incubated with NI01. (A) Topography of NI01-treated SLBs mimicking bacterial membranes (see Methods). (B) Higher magnification images of individual patches (brighter areas) with petal-like pores (darker areas) from (A). The images were taken within the first 10 min of incubation with NI01 (0.25 μM). (C) Height profiles as measured along the highlighted lines in (A) and (B). (D) SLBs imaged at a low magnification, with the framed area imaged at a higher magnification (E) over 1 hour to show growing pores and patches as highlighted by white arrows (from left to right). Colour scale bar is 15 nm. Length scale bars are 500 nm for (A) and (D), 100 nm for (B) and 200 nm for (E).

Figure 4. Membrane poration modes by two-helix hairpins. In liquid AFM topography images of SLBs mimicking bacterial membranes treated with two-helix hairpins derived from NI01. The images were taken within the first 5 min of incubation with each hairpin (0.25 μM). Height profiles are measured along the highlighted lines. Colour scale bar is 15 nm, length scale bars are 500 nm for the low magnification images (left) and 200 nm for the high magnification images (right). The two-helix hairpins are isolated segments of the reported crystal structure.

Figure 5. Comparative behaviour of aureocin A53. (A) Amino-acid sequences of NI01 and A53. Identical amino acids are highlighted in cyan. (B) NMR solution structure of A53 bacteriocin (PDB entry 2N8O rendered by PyMol) (Acedo et al., 2016). (C) CD spectra for NI01 (dashed line) and A53 (black line) (20 μM protein) in 10 mM phosphate buffer. (D) Topography AFM images of anionic SLBs treated with A53 (0.25 μM). (E) A higher magnification image with height profiles measured along the highlighted lines. Colour and length scale bars are 15 nm and 500 nm (D) and 200 nm (E), respectively.

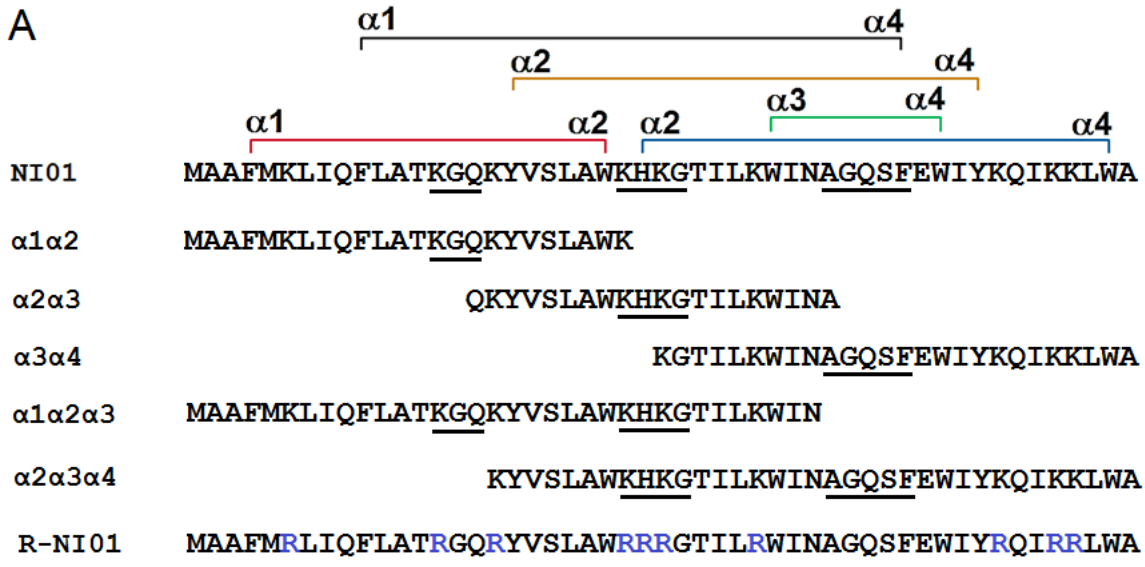
A
α1
α4
α2
α4
α3
α4
α1
α2
α2
α4
NI01 MAAFMKLIQFLATKGQKYVSLAWKHKGTILKWINAGQSFEWIYKQIKKLWA
α1α2 MAAFMKLIQFLATKGQKYVSLAWK
α2α3 QKYVSLAWKHKGTILKWINA
α3α4 KGTILKWINAGQSFEWIYKQIKKLWA
α1α2α3 MAAFMKLIQFLATKGQKYVSLAWKHKGTILKWIN
α2α3α4 KYVSLAWKHKGTILKWINAGQSFEWIYKQIKKLWA
R-NI01 MAAFMRLIQFLATRGQRYVSLAWRRRGTILRWINAGQSFEWIYRQIRRLWA

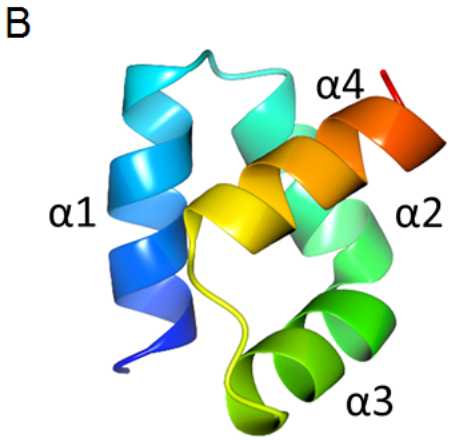
B
α4
α1
α2
α3

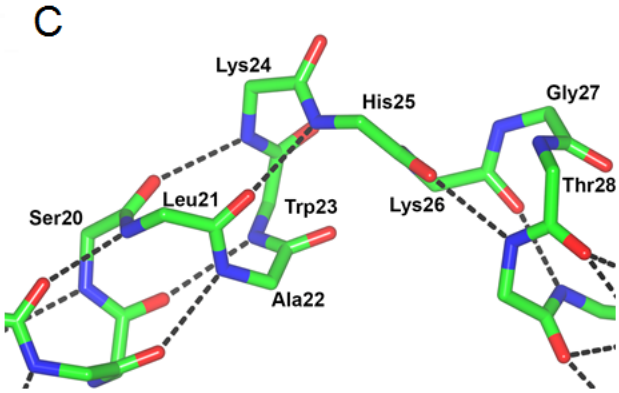
C
Lys24
His25
Gly27
Thr28
Leu21
Trp23
Lys26
Ser20
Ala22

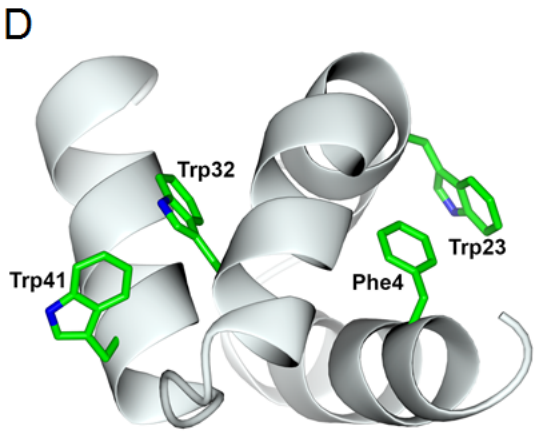
D
Trp32
Trp23
Trp41
Phe4

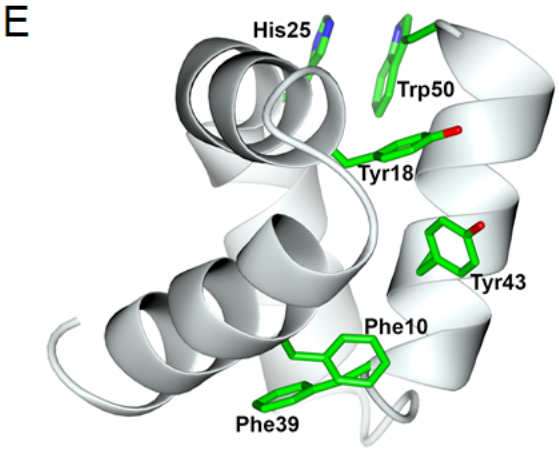
E
His25
Trp50
Tyr18
Tyr43
Phe10
Phe39

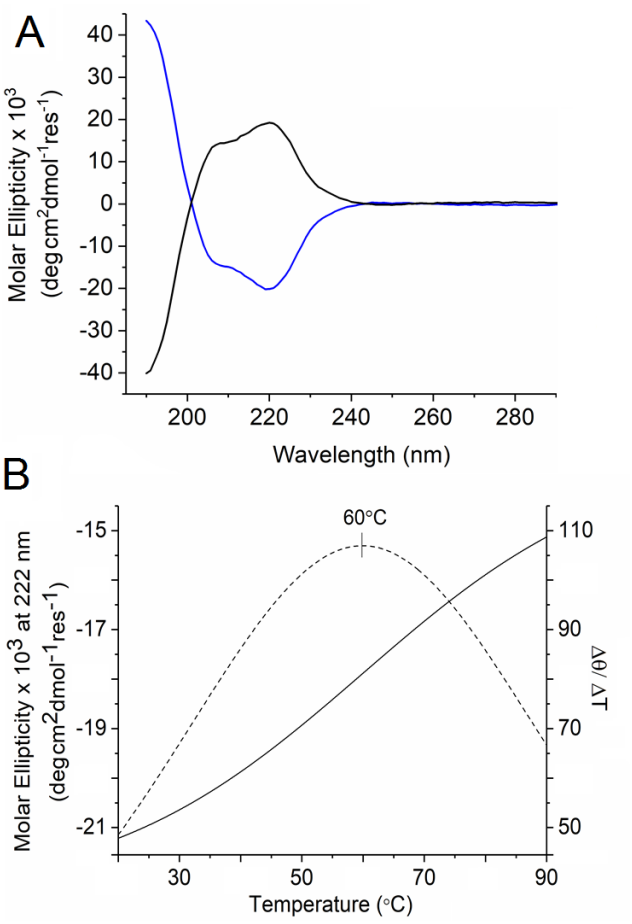
A
Molar Ellipticity x 10^3 (deg cm^2 dmol^-1 res^-1)
Wavelength (nm)
B
60°C
Molar Ellipticity x 10^3 at 222 nm (deg cm^2 dmol^-1 res^-1)
dθ/dT
Temperature (°C)

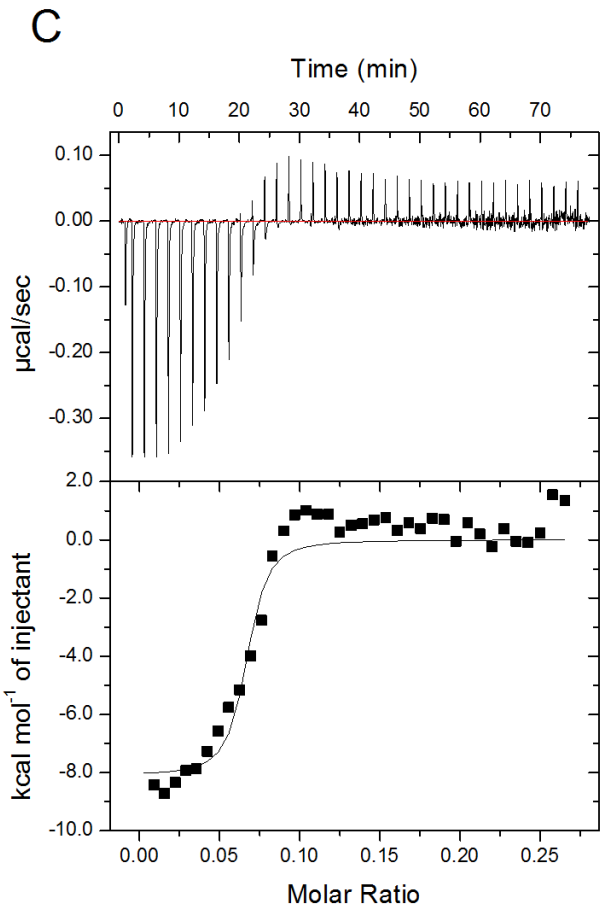
C
Time (min)
µcal/sec
kcal mol^-1 of injectant
Molar Ratio

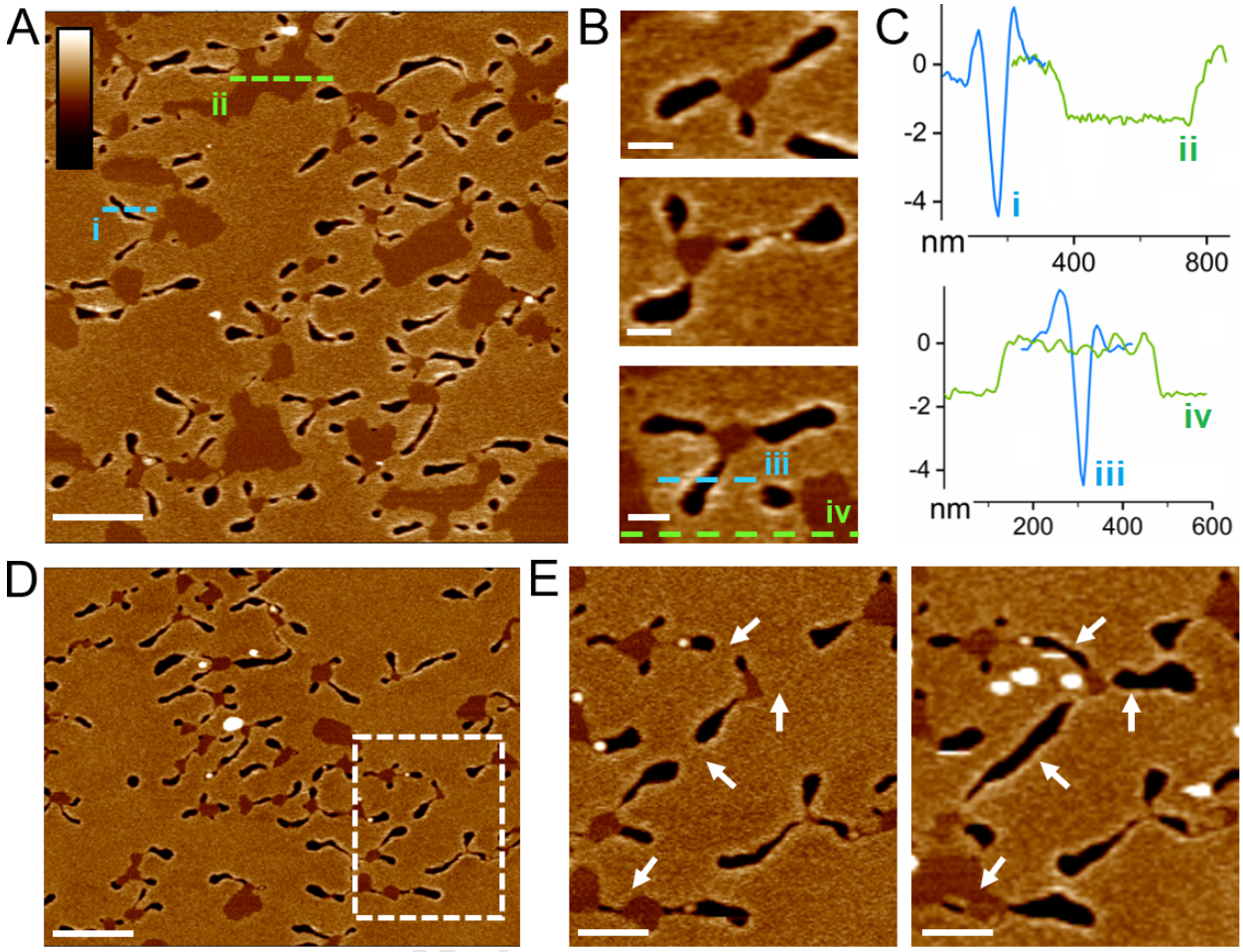

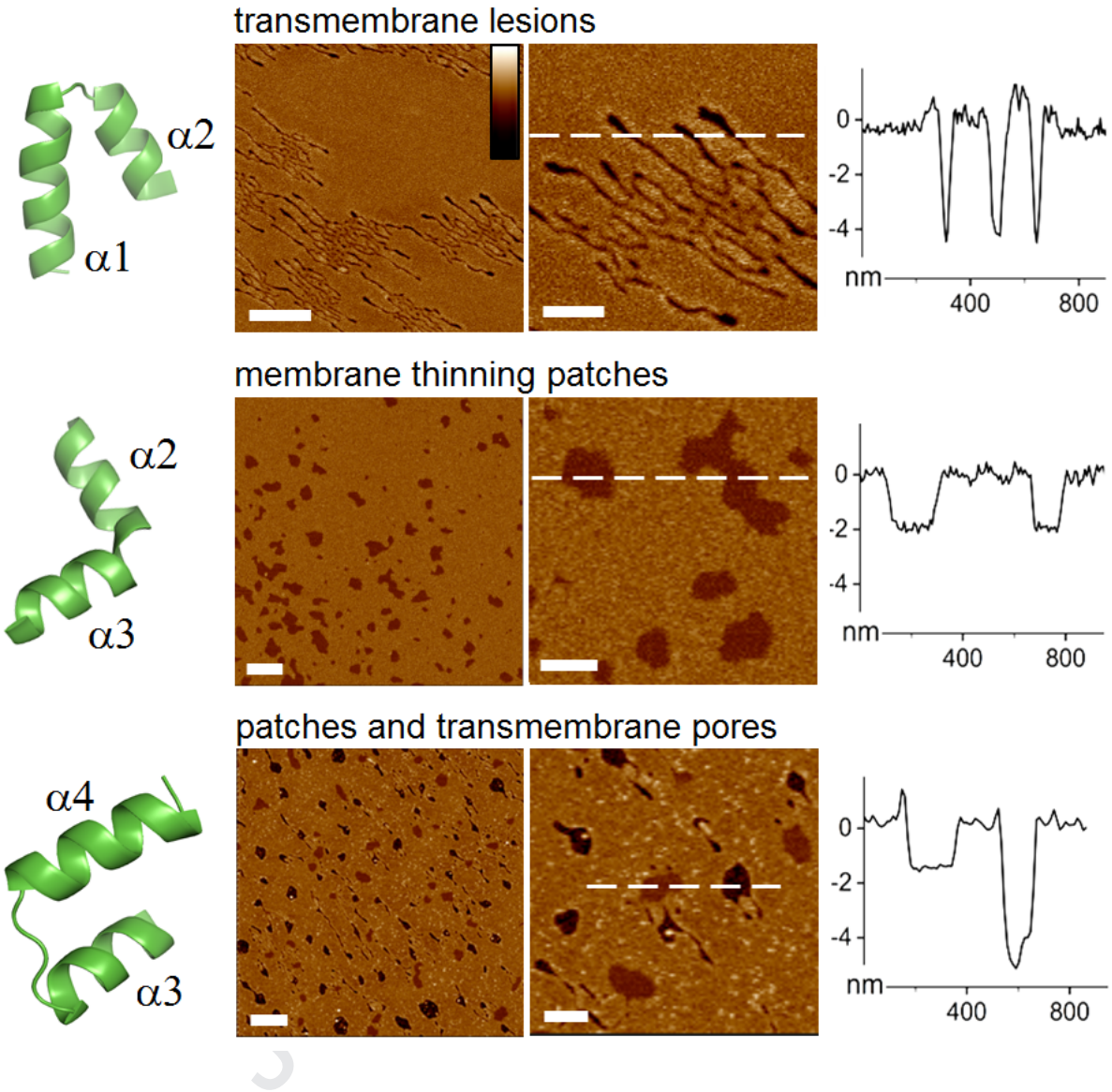
transmembrane lesions
α2
α1
0
-2
-4
nm
400
800
membrane thinning patches
α2
α3
0
-2
-4
nm
400
800
patches and transmembrane pores
α4
α3
0
-2
-4
nm
400
800

A

```
NI01  MAAFMKLIQFLATKGQKYVSLAWKHKGTILKWINAGQSFEWIYKQIKKLWA
A53   M_SWLNFLKYIAKYGKKAVSAAWKYKGKVLEWLNVGPTLEWVWQKLKKIAGL
```

B

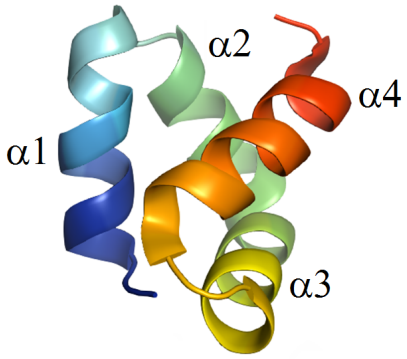

C

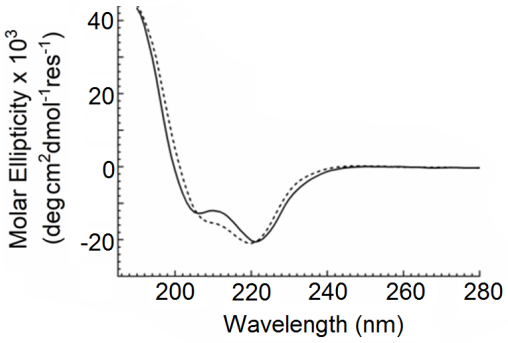

D

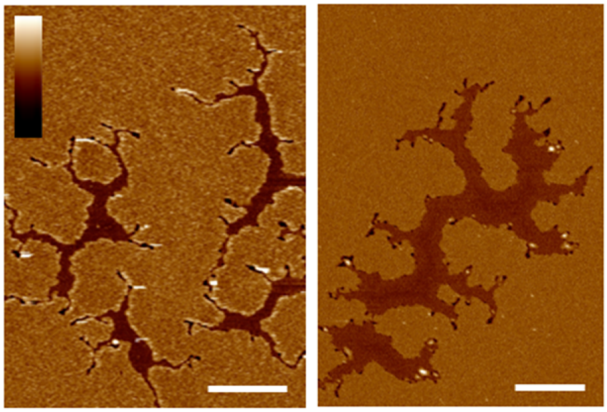

E

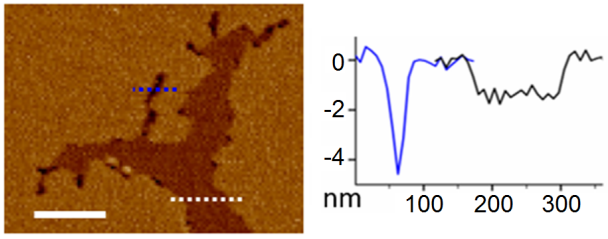

- bacteriocins are antibacterial proteins believed to form pores in bacterial membranes
- a multi-helix bacteriocin fold induces a multi-mode poration mechanism
- each of two-helix segments of the bacteriocin adopts a particular poration mode
- these segments act synergistically balancing out antibacterial and hemolytic activities